Geophysical Journal International

Geophys. J. Int. (2018) **212,** 1331–1343
Advance Access publication 2017 October 24
GJI Seismology

doi: 10.1093/gji/ggx462

Earthquake triggering in southeast Africa following the 2012 Indian Ocean earthquake

Miguel Neves,[1,2] Susana Custódio,[1] Zhigang Peng[2] and Adebayo Ayorinde[2,3]

[1] *Instituto Dom Luiz, Faculdade de Ciências, Universidade de Lisboa, Campo Grande,* 1749-016 *Lisbon, Portugal. E-mail: miguelgneves@gmail.com*
[2] *School of Earth and Atmospheric Sciences, Georgia Institute of Technology, Atlanta, GA* 30332*, USA*
[3] *School of Civil and Environmental Engineering, Georgia Institute of Technology, Atlanta, GA* 30332*, USA*

Accepted 2017 October 20. Received 2017 October 18; in original form 2017 June 23

SUMMARY

In this paper we present evidence of earthquake dynamic triggering in southeast Africa. We analysed seismic waveforms recorded at 53 broad-band and short-period stations in order to identify possible increases in the rate of microearthquakes and tremor due to the passage of teleseismic waves generated by the M_w8.6 2012 Indian Ocean earthquake. We found evidence of triggered local earthquakes and no evidence of triggered tremor in the region. We assessed the statistical significance of the increase in the number of local earthquakes using β-statistics. Statistically significant dynamic triggering of local earthquakes was observed at 7 out of the 53 analysed stations. Two of these stations are located in the northeast coast of Madagascar and the other five stations are located in the Kaapvaal Craton, southern Africa. We found no evidence of dynamically triggered seismic activity in stations located near the structures of the East African Rift System. Hydrothermal activity exists close to the stations that recorded dynamic triggering, however, it also exists near the East African Rift System structures where no triggering was observed. Our results suggest that factors other than solely tectonic regime and geothermalism are needed to explain the mechanisms that underlie earthquake triggering.

Key words: Africa; Earthquake interaction, forecasting and prediction; Seismicity and tectonics.

1 INTRODUCTION

Earthquake–earthquake interactions provide critical insights on the transfer of stress in the lithosphere and on earthquake nucleation processes (Hill & Prejean 2015; King & Devès 2015). Such interactions, of which aftershock sequences are a prime example, have been documented for long (Omori 1894; Utsu *et al.* 1995; Kanamori & Brodsky 2004). In this paper we focus on dynamic triggering—a significant increase of local seismic activity, including earthquakes and tremor, by the dynamic stresses imposed by the passing seismic waves generated by remote large earthquakes, which temporarily alter the local stress field (Hill & Prejean 2015). Dynamic triggering was first convincingly documented in 1992, when the seismicity rate in the western United States conspicuously increased on the wake of the Mw7.3 Landers, California, earthquake (Hill *et al.* 1993). Remote triggering has since been extensively documented elsewhere around the world (Brodsky & van der Elst 2014; Hill & Prejean 2015). Velasco *et al.* (2008) analysed seismic data recorded worldwide following 15 earthquakes of magnitude greater than 7.0 and concluded that dynamic triggering was a widespread phenomenon that took place in various tectonic environments.

Although dynamic triggering has been documented in various tectonic settings, most triggered microearthquakes have been observed in extensional regimes, geothermal areas and volcanic settings (e.g. Aiken & Peng 2014; Hill & Prejean 2015). Recent studies suggest that areas of induced anthropogenic seismicity are also susceptible to remote dynamic triggering (van der Elst *et al.* 2013; Wang *et al.* 2015; Han *et al.* 2017). In comparison, triggered deep tectonic tremor is most commonly observed in compressive and transpressive settings: subduction zones, strike-slip faults and arc-continental collisions (e.g. Peng & Chao 2008; Peng *et al.* 2009; Peng & Gomberg 2010; Aiken *et al.* 2016). Triggered tremor typically shows a sustained increase in high-frequency seismic energy with no clear impulsive phases and is often modulated by the passing surface waves of the teleseismic event (Rubinstein *et al.* 2007; Peng *et al.* 2009).

In dynamic triggering, the onset of the increase in the rate of local seismic activity typically coincides with the passage of the surface wave train, in which case it is referred to as instantaneous dynamic triggering (Hill & Prejean 2015). When the rate of local seismic activity remains abnormally high in the hours to days following the passage of teleseismic waves, it is referred to as delayed dynamic triggering (Parsons 2005; Brodsky 2006; Shelly *et al.* 2011; Castro *et al.* 2015). Although the mechanisms underlying dynamic triggering are not yet completely understood (Brodsky & van der Elst 2014), proposed mechanisms include

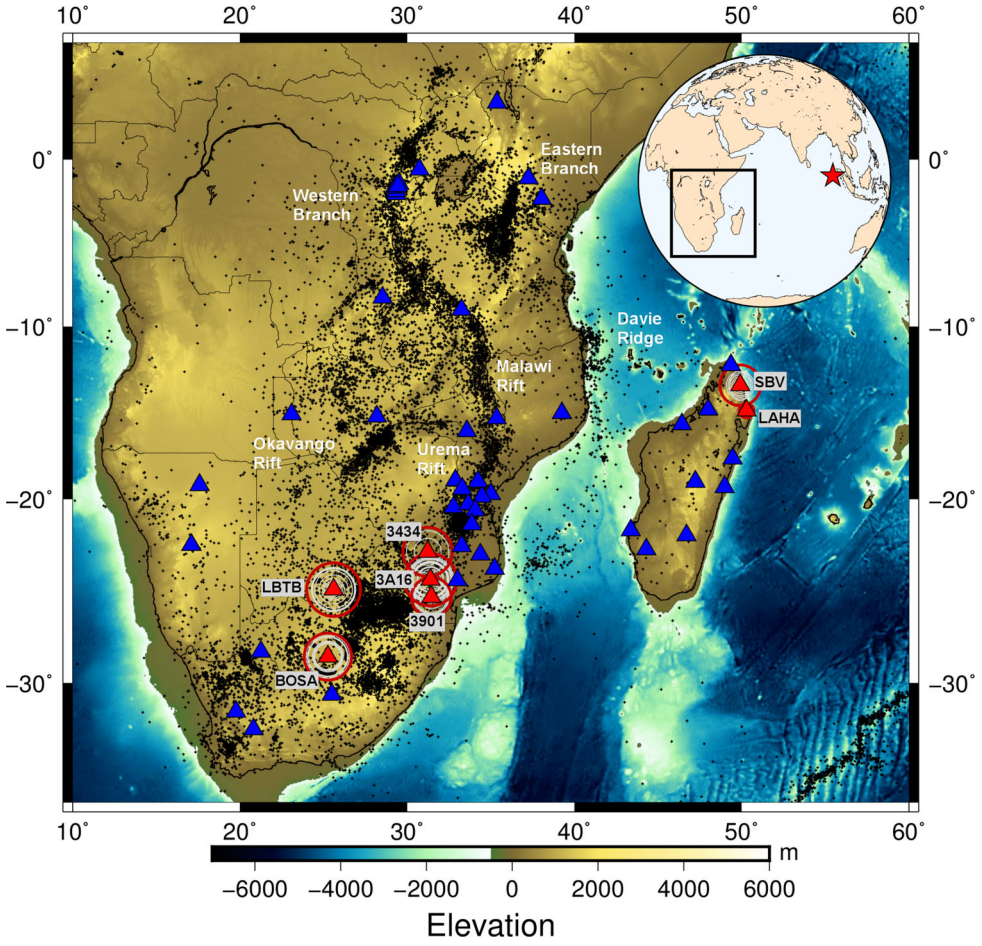

Figure 1. Map of central and south Africa. The small '+' mark the seismicity from 1901 to 2016 (International Seismological Centre 2016). The seismicity clearly defines the structures of the EARS. Clusters of earthquakes in South Africa result both from natural and anthropogenic causes. Blue triangles represent the stations where no significant increase in activity was found. Red triangles represent the stations where remotely triggered earthquakes were observed: two stations in the northeast coast of Madagascar and five stations around one of the South Africa most active clusters. Circles around these stations mark the possible locations of triggered earthquakes computed from *S*–*P* time differences; green and red circles mark the shortest and most distant circles for each station. The location of the M_w8.6 2012 Indian Ocean earthquake (red star) relative to the study area (black square) is shown in the top right inset map.

triggering by frictional failure (Gonzalez-Huizar & Velasco 2011) and triggering through the excitation of crustal fluids (Hill & Prejean 2015).

The April 11, 2012, M_w8.6 Indian Ocean earthquake (08:38:37 UTC)—the largest instrumentally recorded strike-slip earthquake—ruptured a complex sequence of 3–4 orthogonal fault segments (McGuire & Beroza 2012; Meng *et al.* 2012; Yue *et al.* 2012; Wei *et al.* 2013). It was followed by an M_w8.2 aftershock that occurred approximately 2 hr after the main shock. The waves generated both by the main shock and by its aftershocks triggered deep tremor and earthquakes globally (e.g. Pollitz *et al.* 2012; Wu *et al.* 2012; Tape *et al.* 2013; Wang *et al.* 2015; Bansal *et al.* 2016; Chao & Obara 2016).

In this paper, we present the results of the first systematic search for remote triggering in southeast (SE) Africa, including the southern section of the East African Rift System (EARS). In the past, the region has been poorly monitored by seismic networks. We take advantage of the occurrence of the 2012 Indian Ocean earthquake at a time when SE Africa was well monitored by permanent and temporary seismic networks to study the effect of dynamic stresses imposed by teleseismic waves on active fault structures of SE Africa.

2 SOUTHEAST AFRICA

The African continent (Fig. 1) was assembled during the Late Precambrian by the amalgamation of several Archean cratons (Craig *et al.* 2011). Proterozoic mobile belts, which resulted from the Pan-African tectono-thermal event, mark the boundaries between Archean cratons (Craig *et al.* 2011). During the Phanerozoic, Africa remained mostly a stable continent. Currently, east Africa is undergoing active continental rifting along the EARS, which separates the Nubia Plate to the west, from the Somalia Plate to the east. The EARS is characterized at the surface by a succession of adjacent basins controlled by faults, which form subsiding grabens or troughs (Chorowicz 2005). Most earthquakes in southeast Africa are associated with the EARS (Foster & Jackson 1998).

The EARS can be divided in two main branches—the Eastern Branch and the Western Branch (Fig. 1). The Eastern Branch is more active in the north and spreads from the Afar region southwards until the north of Tanzania. The Western Branch separates from the Eastern Branch between Afar and Tanzania, in the Aswa shear zone. It extends from Lake Albert, Uganda, down to the Malawi rift, from where its propagation further south becomes unclear. Different hypothesis for its southward continuation have been proposed: (1) through the Urema Rift in Central Mozambique

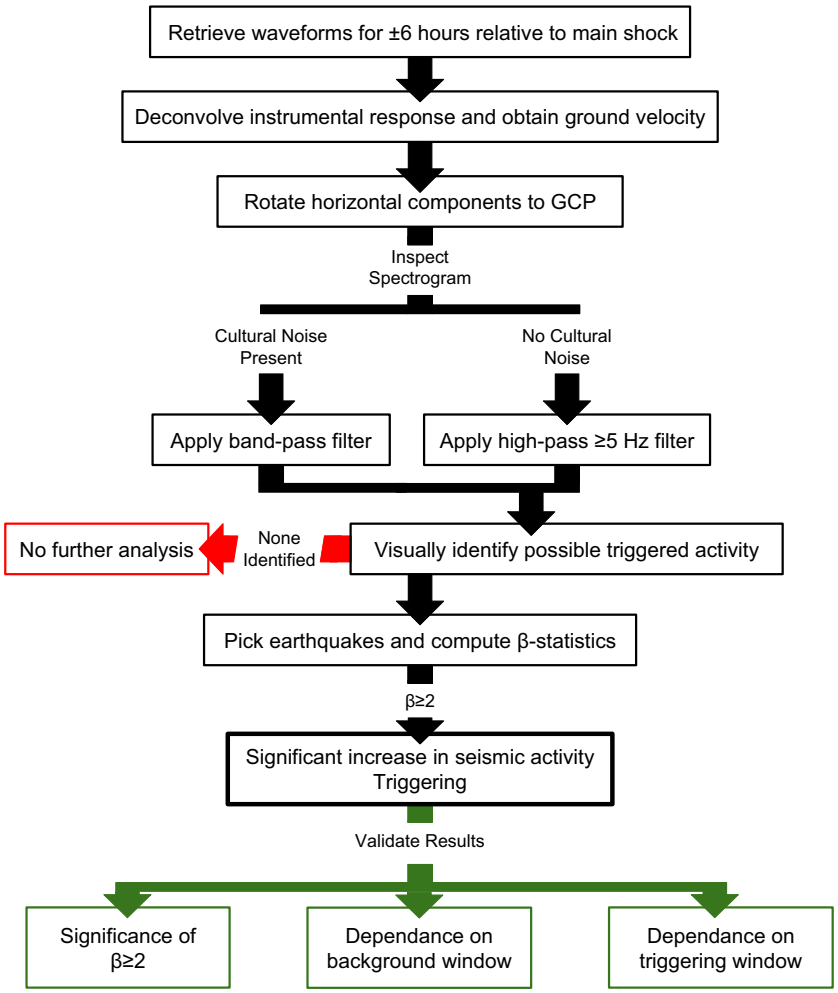

Figure 2. Schematic description of the data processing steps followed in this study. GCP: Great Circle Path.

(Ebinger *et al.* 1987), supported by recent seismological investigations (Fonseca *et al.* 2014; Domingues *et al.* 2016); (2) a bifurcation south of Lake Tanganyika that continues through the Okavango Rift (Scholz *et al.* 1976); (3) a third southeastern branch that spreads offshore through the seismically active Davie Ridge in the Mozambique Channel (Mougenot *et al.* 1986); and (4) a diffuse plate boundary and the existence of several microplates between the Nubia and Somalia plates (Stamps *et al.* 2008), which considers a continuation through Madagascar, possibly through the central Madagascar Alaotra-Ankay rift valley (Kusky *et al.* 2010). The Eastern branch is currently in a more mature stage of the rifting process than the Western branch (Craig *et al.* 2011). It is also shorter and seismic activity along its extent is less common than in the Western Branch, which is seismically active along its entire length (Craig *et al.* 2011). In opposition, Cenozoic volcanism along the EARS is widespread in the north, especially along the eastern branch, but sparse in the south (Chorowicz 2005).

Natural and anthropogenic earthquakes unrelated to the EARS are also documented in southeast Africa, particularly—but not exclusively—in South Africa. A noteworthy natural M6.5 earthquake occurred in Botswana on 2017 April 3. Anthropogenic events have been related to mining and to the impoundment of water in dams (Singh *et al.* 2009). Clusters of moderate magnitude seismicity in central and southwest South Africa have also been associated with geothermal activity (Singh *et al.* 2009).

3 DATA AND METHODS

We inspected data recorded at 53 broad-band and short-period seismic stations in southeast Africa (Fig. 1), including 16 stations from a temporary deployment in Mozambique (Fonseca *et al.* 2014) and 37 openly available seismic stations (networks AF, GE, GT, II, IU, XV, YA). For each station, we analysed the waveforms recorded 6 hr before and after the origin time of the 2012 Indian Ocean earthquake. The detailed data analysis procedure is shown in Fig. 2, and is briefly summarized here.

We first deconvolved the instrumental response and carried out all the analysis using velocity waveforms. When all three-components of ground motion recordings were available, we rotated the horizontal components to transverse and radial (Figs 3b and 4b). In order to suppress the long period energy of teleseismic waves and rather focus on the search for high-frequency local events, we applied a high-pass ($\geq$5 Hz) filter (Figs 3a and c). When cultural noise affected the waveforms in the frequency bands relevant for the analysis, we used band-pass filters to isolate the signals of interest (Figs 4a and c). In these cases, the frequency pass-bands were chosen by visual inspection of spectrograms (Fig. 4d).

We started by visually identifying stations that recorded possible triggered seismic activity during and after the passage of teleseismic waves. We looked both for triggered earthquakes and triggered tremor. We defined triggered earthquakes as those generating signals with clearly distinct *P* and *S* phases above the background noise

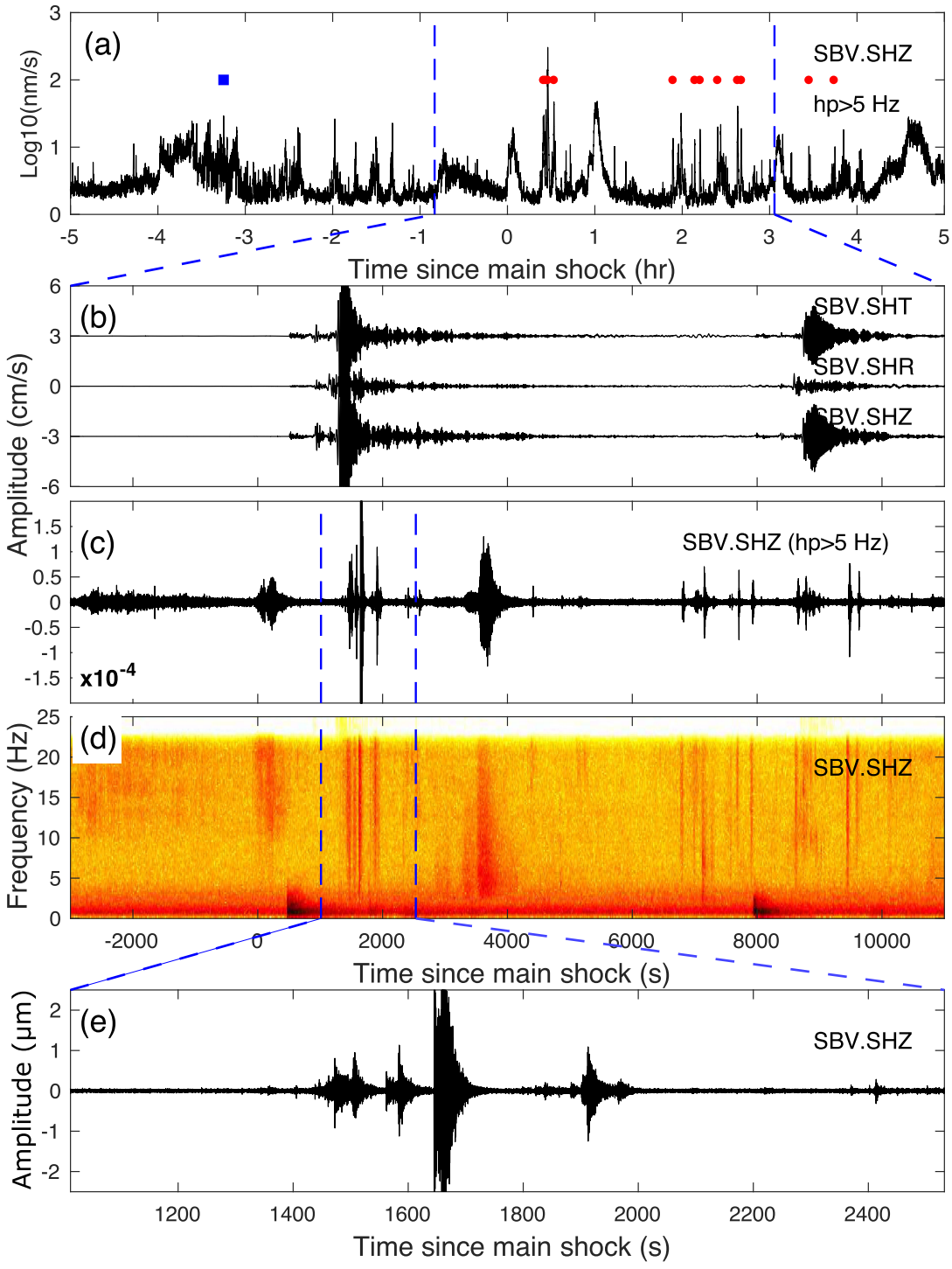

Figure 3. Remote dynamic triggering at station SBV in Madagascar. (a) Envelope of the high-pass filtered (≥5 Hz) vertical velocity recorded in the 6 hr before and after the 2012 M_w8.6 Indian Ocean main shock. Blue squares mark picked events before the instantaneous triggering window and red circles picked events in the triggering windows. (b) Transverse, radial and vertical seismograms during the passage of the main shock and M_w8.2 aftershock. (c) High-pass filtered ≥5 Hz velocity waveform (same time window as in (b). (d) Spectrogram of the vertical velocity waveform (same time window as in (b). (e) Zoom of the band-passed velocity waveform (shown in c) around the time of the main shock surface waves.

level. We only searched for signals with *S*–*P* times <40 s, according to the interstation distances between analysed stations. We defined triggered tremor as generating signals above the background noise level, with longer durations, no clear phase arrivals and modulated by long-period surface waves. In the cases where we visually identified possible triggered activity, we assessed the significance of the rate of change of seismic activity using β-statistics (Aron & Hardebeck 2009). We manually identified and picked earthquakes in the 12 hr of analysed data. We then computed the β-value to compare the number of events that occurred in a time window after the arrival of teleseismic waves with the number of events that would be expected in the same time window using the background

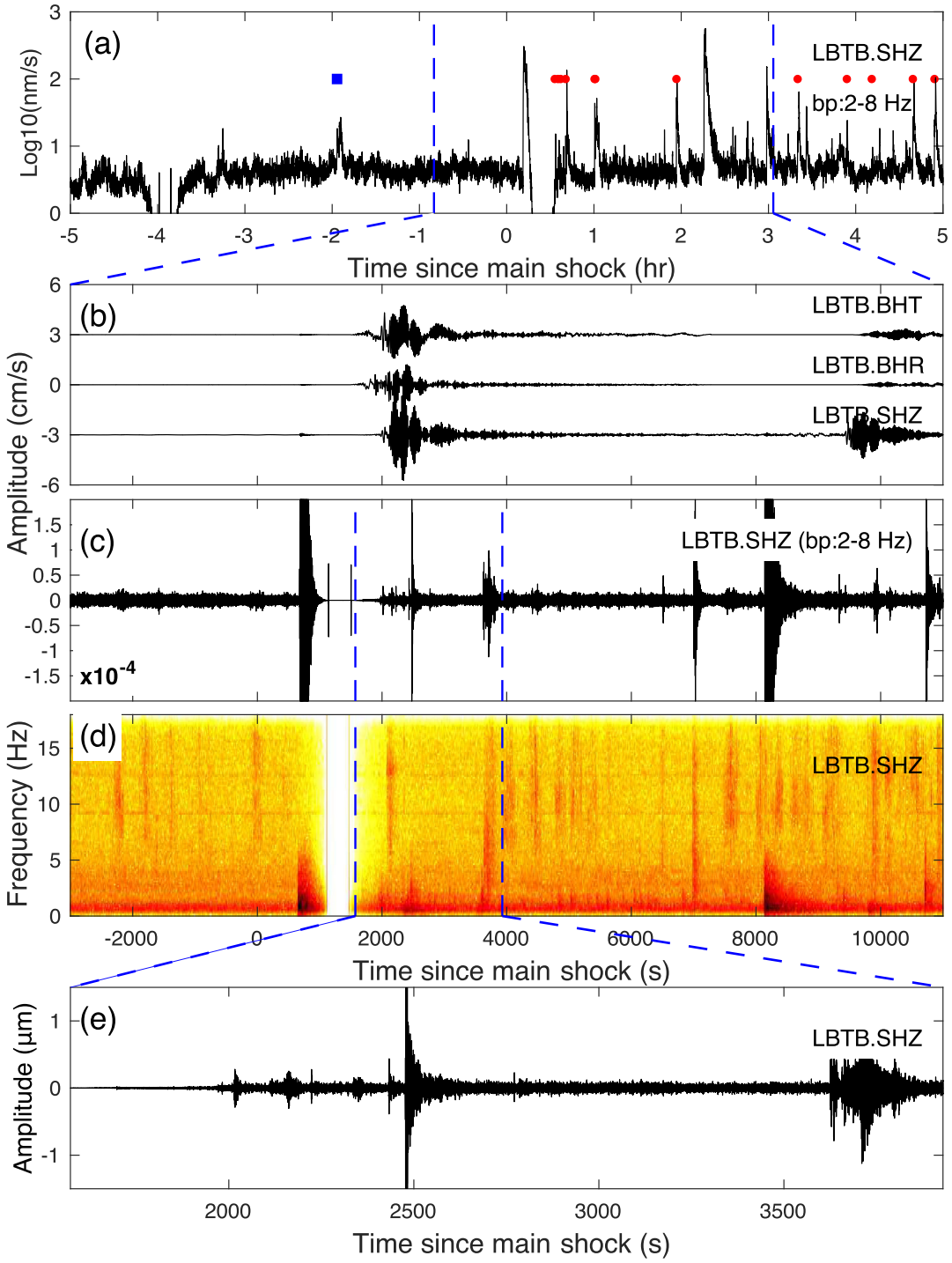

Figure 4. Remote dynamic triggering at station LBTB in Southern Botswana. Same figure caption as for Fig. 3, except now the waveforms were band-pass filtered (2–8 Hz) due to the strong cultural noise above 8 Hz.

seismicity rate estimated based on the 6 hr of data recorded before the arrival of the teleseismic *P*-wave arrival. The β-value is calculated as follows:

$$\beta = \frac{N_a - N(T_a/T)}{\sqrt{N(T_a/T)(1-(T_a/T))}} \quad (1)$$

where T_a is the time length of the triggering window, T is the time length of the background seismicity window plus the triggering window, and N_a and N are the number of events detected in T_a and T, respectively. A statistically significant increase in the rate of seismic activity is found when $\beta \geq 2$ (Hill & Prejean 2015). We defined two consecutive triggering windows to search for both instantaneous and delayed triggering. The instantaneous triggering window encompasses the passage of surface waves, estimated as the time between the arrival of seismic energy travelling at 5 and 2 km s^{-1} (Peng *et al.* 2009). The delayed triggering window extends from the end of the instantaneous triggering window up until 6 hr after the main shock's origin time (Aiken & Peng 2014). The

Table 1. β-values computed for the 10 stations with a visually detected increase in earthquake rate during or after the passage of the Indian Ocean earthquake teleseismic waves. T_b indicates the length of the background window, 6 or 24 hr before the main shock until the teleseismic *P*-wave arrival. Underlined values identify $\beta \geq 2$, suggesting statistically significant triggering.

T_b (hr)		3434	3901	3A16	BOSA	KIBK	LBTB	LAHA	MBAR	SBV	UPI
6	β_i	5.03	4.52	3.55	4.01	−0.50	6.85	4.88	0.91	6.02	0.99
6	β_d	3.60	1.86	3.62	1.48	1.88	2.70	2.14	0.29	2.14	0.71
24	β_i	8.97	6.91	3.00	5.67		7.87	5.92		10.51	

Note. β_i, instantaneous triggering window; β_d, delayed triggering window.

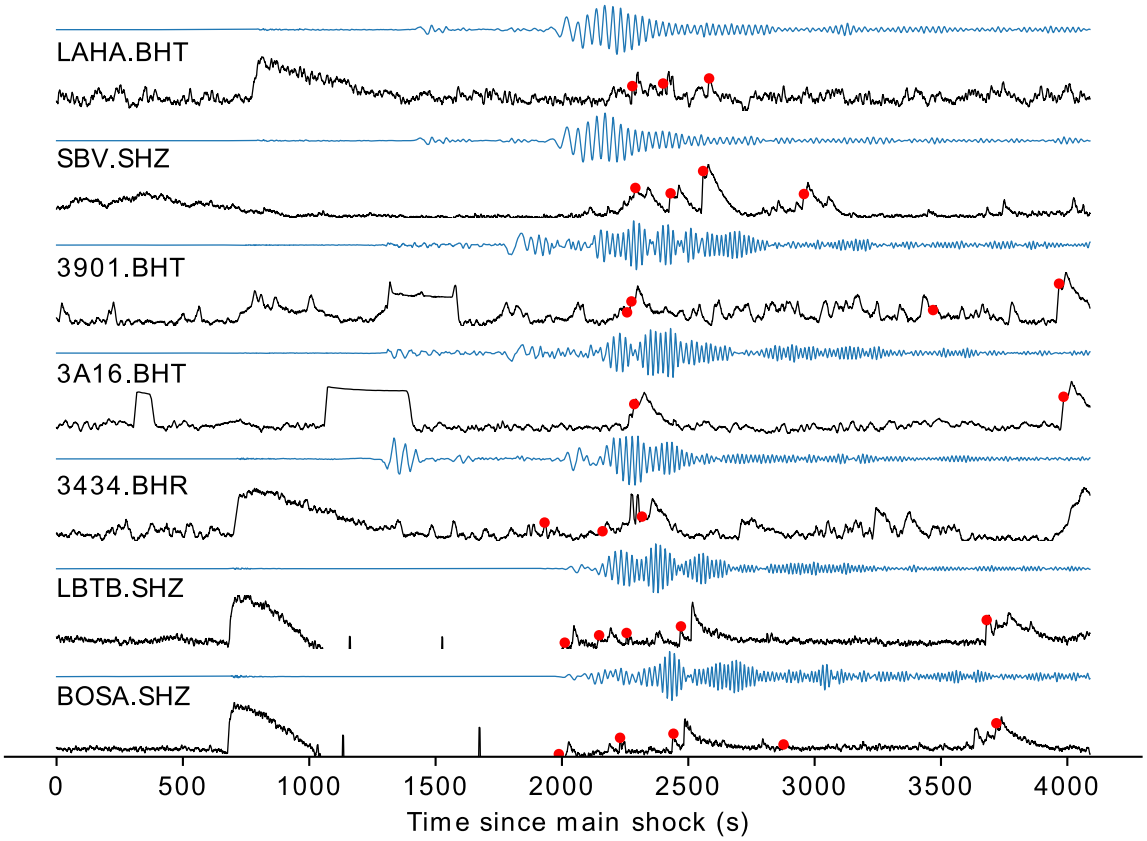

Figure 5. M_w8.6 2012 Indian Ocean main shock surface wave train (light blue) recorded in the seven stations that presented a statistically significant increase in the rate of seismic activity. The envelopes of the corresponding filtered waveforms are shown in black. The dynamically triggered local microearthquakes that were manually identified are marked as red dots. For stations 3434, 3901 and LBTB, we applied a band-pass filter of 2–8 Hz. For the other 4 stations we applied a high-pass filter of ≥5 Hz.

background seismicity rate was computed considering the time window extending from 6 hr before the main shock until the teleseismic *P*-wave arrival.

For those stations where the β-statistics analysis revealed a significant ($\beta \geq 2$) increase in seismic activity, we further investigated the robustness of triggering. To this end, we retrieved waveforms recorded 24 hr before and after the origin time of the main shock. We then identified and picked earthquakes in the 48 hr of data and performed three additional tests with the new catalogues:

(i) *Significance of $\beta > 2$*. We defined a moving triggering window with the length of the instantaneous triggering window sweeping along the 48 hr of data. For each second of data we compared the triggering window to the background window and calculated the respective β-value. We then assessed which sections of our catalogue presented $\beta \geq 2$ and whether the increase in seismic activity during the passage of the surface waves was significant. The background seismicity rate was estimated from a fixed time window extending from 24 hr before the main shock until the teleseismic *P*-wave arrival.

(ii) *Dependence on background window*. We randomly chose 1000 background window lengths, varying between 1 to 24 hr, and for each computed the β-value with the window starting at 1000 different times in the 24 hr before the main shock. We considered the same instantaneous triggering window as in the original β-statistics analysis (time between the arrival of seismic energy traveling at 5 and 2 km s^{-1}). We then analysed the distribution of β-values to assess whether the increase in seismic activity was independent of the chosen background window.

(iii) *Dependence on triggering window.* We also calculated the β-value for an increasing length of the considered triggering window. Starting with the instantaneous triggering window, we calculated β-values for triggering windows with successive additional 1 s until 24 hr after the main shock. We defined the background window starting at 24 hr before the main shock and ending at the teleseismic *P*-wave arrival.

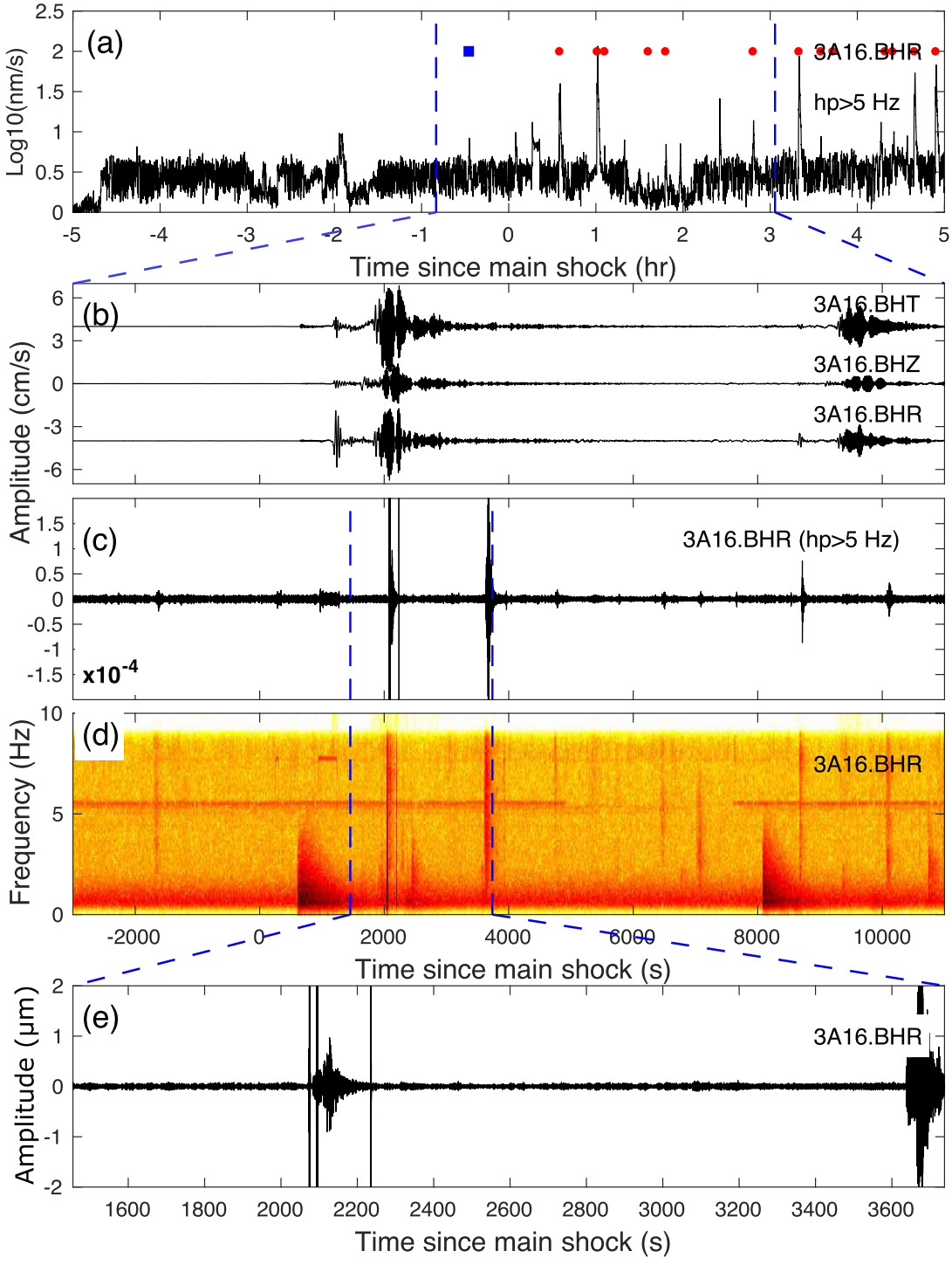

Figure 6. Remote dynamic triggering at station 3A16 in southern Africa. Same figure caption as for Fig. 3.

4 RESULTS

The visual inspection of data recorded at the 53 stations resulted in the identification of 10 stations with enhanced microearthquake activity during or after the passage of teleseismic waves. We found no evidence of triggered tremor. Most stations affected by strong cultural noise recorded high-amplitude seismic energy at frequencies above 10 Hz. In these cases, we applied a bandpass filter of 2–8 Hz in order to eliminate the cultural noise. Fig. 4(d) shows an example of a station (LBTB) affected by cultural noise that is particularly intense at 10–15 Hz. In those cases where noise was very strong in the frequency band of interest to our analysis (2–8 Hz), we did not use the station for further analysis. Table 1 shows the β-values computed for the instantaneous and delayed triggering windows. Seven out of the ten stations presented a statistically significant increase ($\beta \geq 2$) in the rate of seismic activity (Fig. 5). Two are located in north Madagascar and the remaining five are located in the Kaapvaal craton, South Africa (Fig. 1).

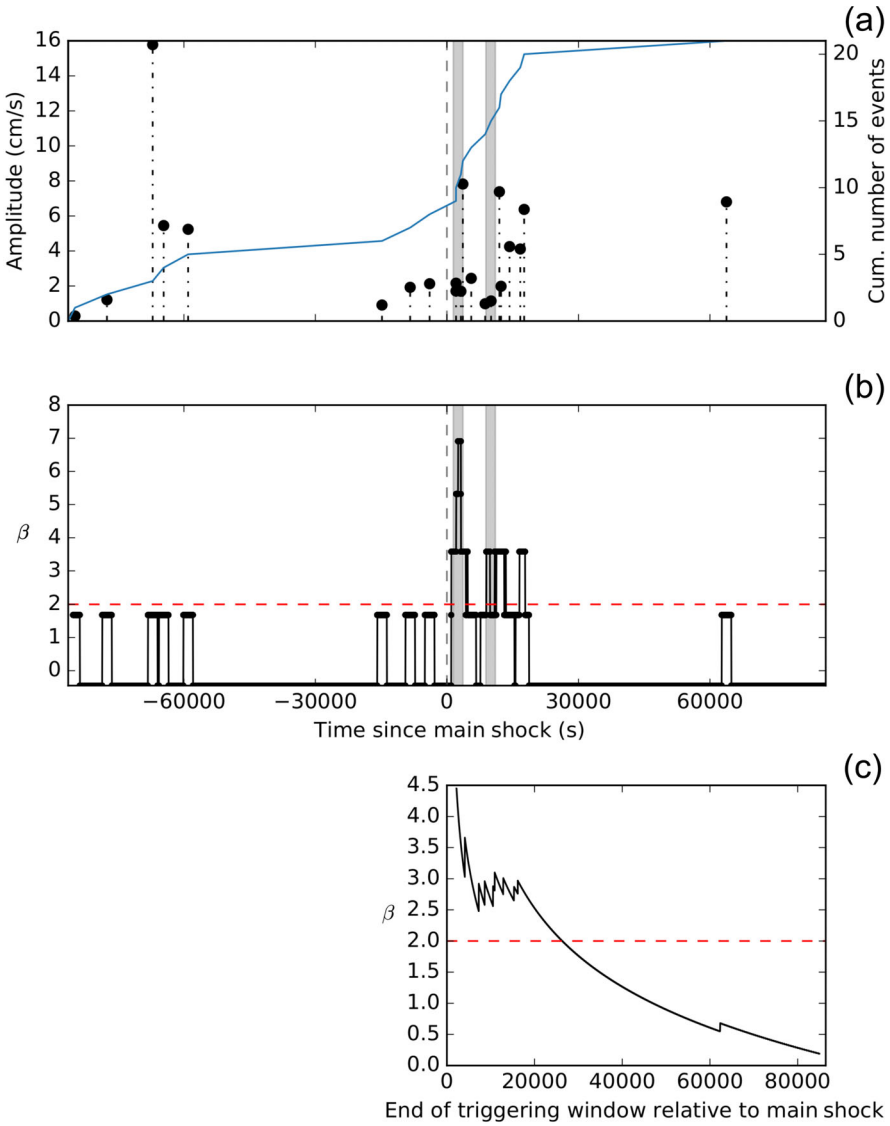

Figure 7. Additional tests performed to validate the significance of triggering for station 3901 in southern Africa. (a) Hand-picked earthquakes in the 24 hr before and after the main shock with the respective amplitudes (*P*-wave PGV) and cumulative number of events (blue line). The vertical dashed grey line marks the origin time of the main shock. The two shaded windows mark the approximate surface wave window (5-2 km s^{-1}) of the 2012 M_w8.6 Indian Ocean main shock and its M_w8.2 aftershock. (b) Results of the significance of $\beta \geq 2$ test. Only the time periods around the passage of the main shock and aftershock result in $\beta \geq 2$ values. The horizontal dashed red line marks $\beta = 2$. (c) Dependence on triggering window test, showing a decay of β-values as the triggering window length increases. The results show also a relative maximum around the time of passage of the seismic waves of the aftershock. These results suggest that the observed increase in the rate of seismic activity results from the dynamic stresses imposed by passing main shock and aftershock seismic waves.

4.1 Triggered seismic activity

4.1.1 Madagascar

We found evidence of locally triggered earthquakes in the northeast coast of Madagascar, at stations LAHA and SBV (Fig. 5). Fig. 3 shows the triggered earthquakes recorded at station SBV. Local earthquakes are recorded during the passage of Rayleigh waves of the M_w8.6 Indian Ocean earthquake and continue to be recorded even after the end of the surface wave train. The β-statistics analysis confirms the significance of the increase in seismic activity both during and after the passage of surface waves at station LAHA (Table 1). Both at station SBV and LAHA, the recorded activity is stronger during the passage of the main shock and of the M_w8.2 aftershock surface waves. At station SBV, we detected 4 microearthquakes during the passage of the main shock Rayleigh wave and 3 during the passage of the aftershock Rayleigh wave. At LAHA, we detected three microearthquakes during the passage of the main shock Rayleigh wave, two microearthquakes during the passage of the aftershock Love wave and three microearthquakes during the passage of the aftershock Rayleigh wave.

The limited data set precludes a robust location of the detected microearthquakes. The *S*–*P* time differences of triggered earthquakes range between 0.5 s and 36 s. If we assume nominal crustal *P*- and *S*-wave velocities of 6 km s^{-1} and 3.45 km s^{-1}, respectively, the corresponding epicentral distances range between 4 km and 265 km (Fig. 1).

4.1.2 Southern Africa

We found a significant increase in the rate of recorded local earthquakes at five stations located in the Kaapvaal Craton: LBTB,

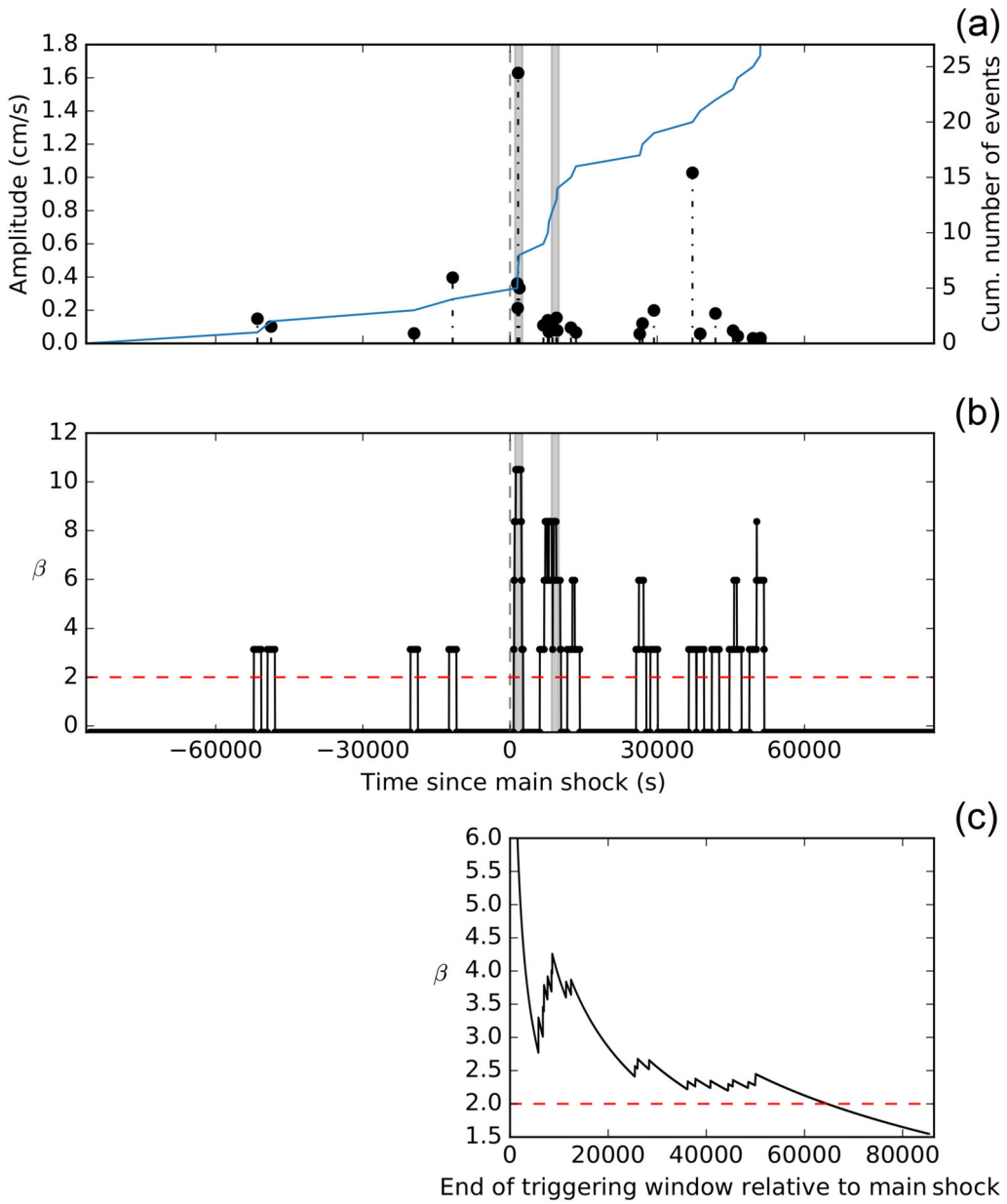

Figure 8. Same caption as for Fig. 7, now for station SBV in Madagascar. (b) A $\beta \geq 2$ is observed at times before the arrival of the main-shock seismic waves. However, these β-values are smaller than the ones observed during the instantaneous triggering window and during the passage of the aftershock seismic waves, confirming that the observed increase in seismic activity with the passage of teleseismic waves is robust.

southeast Botswana; BOSA, central South Africa; and 3A16, 3434 and 3901, in the border between South Africa and Mozambique, near the Lebombo monocline. The increase in seismic activity at stations LBTB (Fig. 4), 3434 and 3A16 (Fig. 6) is statistically significant both in the instantaneous and delayed triggering windows (Table 1). At stations BOSA and 3901 the increase is only significant during the passage of surface waves (Table 1). The onset of the increase in the rate of seismic activity occurs during the passage of the main shock surface waves at all stations except 3434 (Fig. 5). At this station, the increase of seismic activity in the instantaneous triggering window is due to a microearthquake recorded before the actual arrival of the surface wave train. Fig. 4 shows an example of the triggered seismic activity at station LBTB. The onset of seismic activity is detected during the passage of the Rayleigh wave at stations LBTB, 3901 and 3A16 and during the passage of the Love wave at station BOSA. The *S–P* times of the local events range between 1 s and 40 s, indicating epicentral distances between 9 and 325 km (Fig. 1).

4.2 Additional tests for triggering

The additional tests performed for these stations support a significant increase in seismic activity during the passage of teleseismic surface waves: (1) When considering a longer background window of 24 hr, the β-values increased (Table 1). (2) The significance of $\beta \geq 2$ test (Figs 7b and 8b) showed that, for most stations, parts of the catalogue in the background 24 hr also generate β-values$\geq$2, for example, stations 3434 (maximum β of 4.52), 3A16 (3.00), BOSA (3.29), LAHA (4.00), LBTB (5.37) and SBV (3.14). Nonetheless, these β-values are smaller than those determined for the

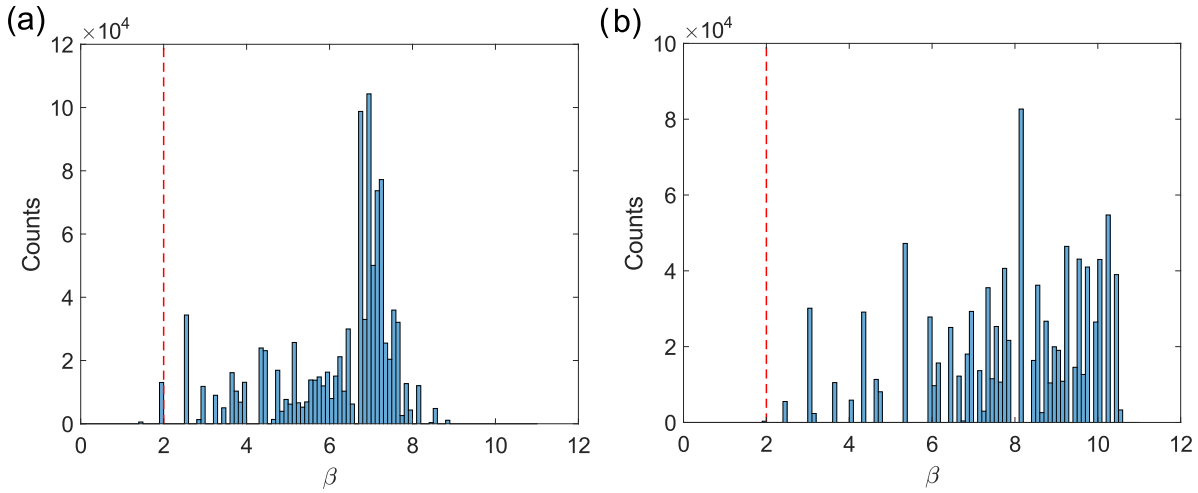

Figure 9. Distribution of β-values determined by dependence on background window test, for station: (a) 3901 in southern Africa; (b) SBV in Madagascar. Most β-values are higher than 2 (vertical dashed red line), indicating that the observed increase in seismic activity is statistically significant.

instantaneous triggering window—by a difference of at least 2—and for the window that encompasses the waves of the M_w8.2 aftershock, except for station 3A16. These results confirm a statistically significant increase in seismic activity during the passage of teleseismic waves. It further suggests that we cannot define a single β threshold for the whole study region. (3) The dependence on background window test (Figs 9a and c) showed that most determined β-values remain higher than 2 independent of background window. (4) Finally, we observed a decay of β with an increasing triggering window (Figs 7c and 8c). At most stations, a relative maximum is also observed around the time of the passage of the M_w8.2 aftershock surface waves. These results indicate that the observed increase in the rate of seismic activity is connected to the dynamic stresses imposed by the passing seismic waves of the Indian Ocean main shock and aftershock.

4.3 Absence of triggering along the southern East African Rift System

Twenty-three of the 53 analysed stations are located near active structures of the EARS. Surprisingly, we found no evidence of triggered tremor or local earthquake activity at these stations during the passage of seismic waves generated by the M_w8.6 Indian Ocean earthquake and its M_w8.2 aftershock (Fig. S1). The visual inspection of waveforms recorded at stations KIBK and MBAR (Fig. S2) revealed a possible increase in seismic activity after the passage of surface waves, but the β-statistics analysis showed that the increase was not statistically significant (Table 1).

5 DISCUSSION AND CONCLUSION

We systematically searched for dynamically triggered seismic activity in southeast Africa following the M_w8.6 2012 Indian Ocean earthquake. We found evidence of local earthquakes triggered in two different regions: the northeast coast of Madagascar and the Kaapvaal craton, central-east South Africa. No evidence was found for the triggering of seismic activity in structures associated with the East African Rift System.

Two of the eleven stations in Madagascar—SBV and LAHA—recorded a statistically significant increase in earthquake rate. The two neighbouring stations are located in the northeast coast of Madagascar, in a region where some seismic activity has been previously reported (Bertil & Regnoult 1998; International Seismological Centre 2016). In particular, an m_b5.0 earthquake was recorded in this region in 1992. Bertil & Regnoult (1998) identify a major reactivated fault, the Nosy-Be Antongil fracture, which is associated with current seismic activity. This fault is located approximately 100 km SW of station LAHA and 200 km S of station SBV. The region is also known for its geothermal activity (Bertil & Regnoult 1998). Because we were not able to locate the detected earthquakes, we cannot clearly associate the triggered earthquakes with structures in the region.

It is intriguing to note that we found evidences of triggering in the northeast coast of Madagascar and not in other regions of Madagascar considered more seismically active, such as in the central Madagascar Alaotra-Ankai rift system (Kusky *et al.* 2010). This observation suggests that faults along the northeast coast of Madagascar may be more easily perturbed by transient dynamic stresses.

Five stations located in the Kaapvaal Craton, central-east South Africa, recorded a significant increase in earthquake rate. Earthquake catalogues show active seismicity in this region, which has been attributed to a combination of natural and anthropogenic factors (Singh *et al.* 2009). Stations 3434, 3901 and 3A16 are located near the Lebombo monocline, which marks the eastern border of the Kaapvaal Craton. The region of the Lebombo monocline hosts low-level background seismic activity (Singh *et al.* 2009). The detected local earthquakes were observed at most in two stations and therefore we could not locate them robustly. We verified that the observed increase in the rate of seismic activity was not related with mining working hours by assessing the level of seismic activity in the same period of time in the 10 days before the main shock. We did not find a similar pattern of increase in the rate of seismic activity in the days before the main shock. We also did not find other time periods with a similar rate of seismic activity as that observed during the passage of teleseismic waves. This result may corroborate previous indications that areas of anthropogenic seismic activity are more prone to remote dynamic triggering (van der Elst *et al.* 2013; Wang *et al.* 2015; Han *et al.* 2017).

It is interesting to note the existence of hydrothermalism close to all stations that recorded dynamic triggering. Hot springs can be found in Madagascar (Bertil & Regnoult 1998), close to the stations that detected triggered activity (Fig. 1). Singh *et al.* (2009)

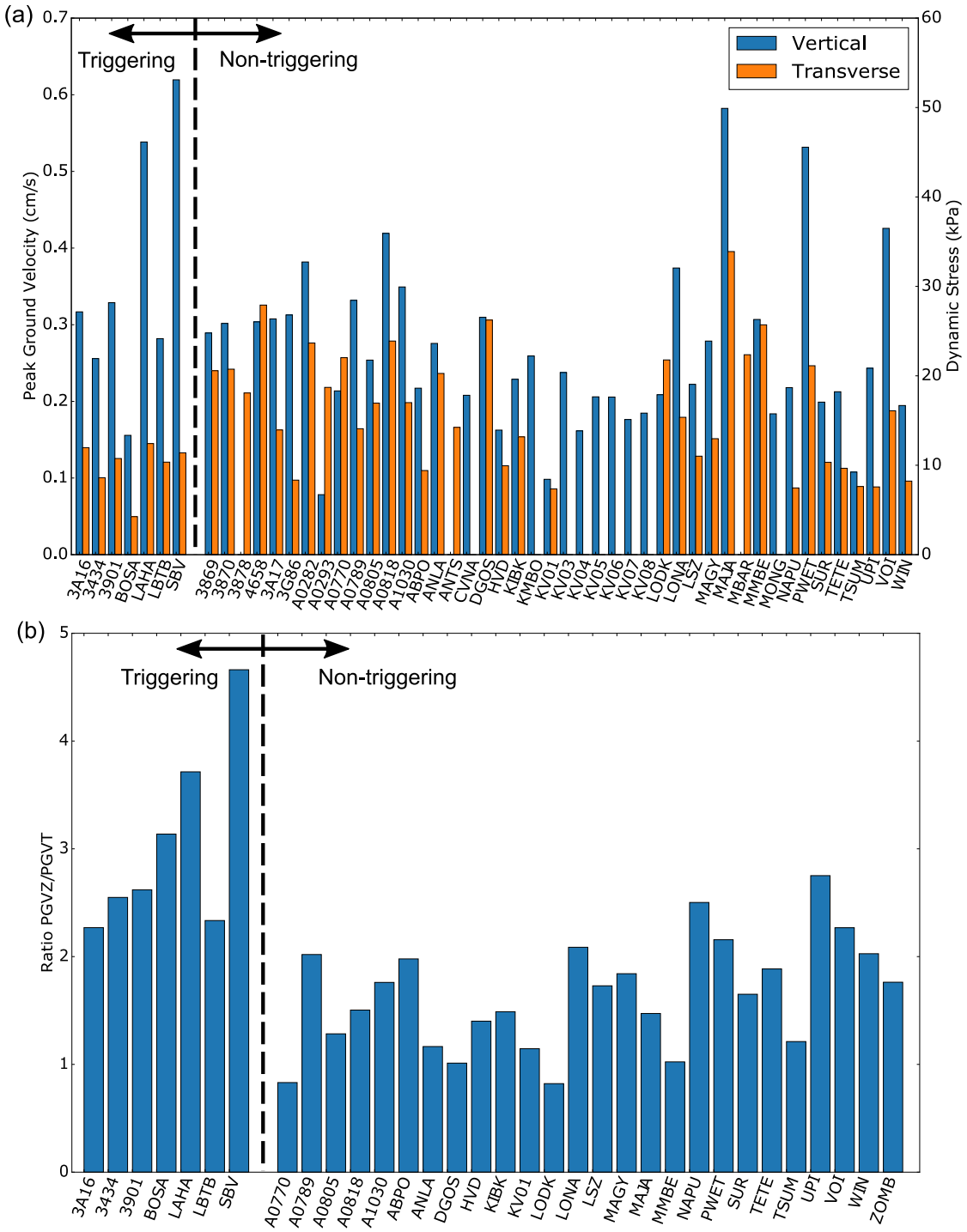

Figure 10. (a) PGV and corresponding dynamic stress recorded on the vertical and transverse components of velocity waveforms in the study region. (b) Ratio between vertical and transverse PGV. A clear relationship between observed PGV and dynamic triggering does not exist. However, stations where triggered earthquakes were recorded appear to present a higher vertical to horizontal ratio PGV. Stations not shown in the graph present anomalous peak ground velocity values and were not considered in the analysis. The dynamic stress was estimated assuming a shear rigidity of 30 GPa and a phase velocity of 3.5 km s^{-1}, following Aiken & Peng (2014).

reported hydrothermalism associated with the Zebediela fault, located in the region of the 5 stations that detected dynamic triggering in the Kaapvaal craton. However, it should be noted that hydrothermalism is also common in other regions of southeast Africa, including close to structures of the EARS, where no triggering was observed.

The absence of triggered earthquakes near the extensive structures of the EARS confirms that dynamic triggering is not ubiquitous along major plate-boundary fault-systems (e.g. Bansal *et al.* 2016). It also suggests that tectonic regime and geothermalism cannot solely explain remote dynamic triggering mechanisms. Other

factors, such as local crustal stress field or pore pressure, should also be considered (Zhang *et al.* 2017).

Fig. 10(a) shows the peak ground velocity (PGV) observed at each station during the passage of teleseismic waves. A clear relationship between surface wave PGV and dynamic triggering does not exist. However, stations where triggering was observed present a high vertical PGV in comparison to the horizontal PGV (Fig. 10b). The high vertical to horizontal PGV ratio suggests a local distortion of the wavefield, possibly due to topography, structure or site effects, which may facilitate triggering.

Finally, our extensive β-statistic tests suggest that a β-value larger than 2 should not be taken as a universal value for determining a significant increase in the rate of seismic activity. The results also indicate that a single β threshold cannot be determined for the study region and that individual thresholds should be considered for different stations.

ACKNOWLEDGEMENTS

We thank the MOZART (MOZAmbique Rift Tomography) project for making available the data from the deployment in Mozambique. Seismic data used in this study are available from the Incorporated Research Institutes for Seismology (IRIS) Data Management Center (AF, doi:10.7914/SN/AF; GT, doi:10.7914/SN/GT; II, doi:10.7914/SN/II; IU, doi:10.7914/SN/IU; XV, doi:10.7914/SN/XV_2011; YA, doi:10.7914/SN/YA_2012) and the GEOFON Data Centre (GE, doi:10.14470/TR560404). The seismic catalogue used in this work was retrieved from the International Seismological Centre (2016). We thank Chenyu Li for providing the MATLAB scripts used to create Figs 3, 4 and 6. The following software packages were used in this study: Seismic Analysis Code (SAC; Goldstein *et al.* 1998), ObsPy (Beyreuther *et al.* 2010) and Generic Mapping Tools (GMT; Wessel & Smith 1998). This work was supported by the Portuguese Science and Research Foundation—Fundação Portuguesa para a Ciência e Tecnologia (FCT) through project SPIDER (PTDC/GEO-FIQ/2590/2014). Zhigang Peng is partially supported by NSF grant EAR-1543399.

REFERENCES

Aiken, C. & Peng, Z., 2014. Dynamic triggering of microearthquakes in three geothermal/volcanic regions of California, *J. geophys. Res.,* **119**(9), 6992–7009.

Aiken, C., Chao, K., Gonzalez-Huizar, H., Douilly, R., Peng, Z., Deschamps, A., Calais, E. & Haase, J.S., 2016. Exploration of remote triggering: A survey of multiple fault structures in Haiti, *Earth planet. Sci. Lett.,* **455,** 14–24.

Aron, A. & Hardebeck, J.L., 2009. Seismicity rate changes along the Central California Coast due to stress changes from the 2003 M 6.5 San Simeon and 2004 M 6.0 Parkfield Earthquakes, *Bull. seism. Soc. Am.,* **99**(4), 2280–2292.

Bansal, A.R., Yao, D., Peng, Z. & Sianipar, D., 2016. Isolated regions of remote triggering in South/Southeast Asia following the 2012 M_w8.6 Indian Ocean earthquake, *Geophys. Res. Lett.,* **43**(20), 10 654–10 662.

Bertil, D. & Regnoult, J.M., 1998. Seismotectonics of Madagascar, *Tectonophysics,* **294**(1–2), 57–74.

Beyreuther, M., Barsch, R., Krischer, L., Megies, T., Behr, Y. & Wassermann, J., 2010. ObsPy: a Python toolbox for seismology, *Seismol. Res. Lett.,* **81**(3), 530–533.

Brodsky, E.E., 2006. Long-range triggered earthquakes that continue after the wave train passes, *Geophys. Res. Lett.,* **33,** L15313, doi:10.1029/2006GL026605.

Brodsky, E.E. & van der Elst, N.J., 2014. The uses of dynamic earthquake triggering, *Annu. Rev. Earth Planet. Sci.,* **42**(1), 317–339.

Castro, R.R., González-Huízar, H., Ramón Zúñiga, F., Wong, V.M. & Velasco, A.A., 2015. Delayed dynamic triggered seismicity in Northern Baja California, México caused by large and remote earthquakes, *Bull. seism. Soc. Am.,* **105**(4), 1825–1835.

Chao, K. & Obara, K., 2016. Triggered tectonic tremor in various types of fault systems of Japan following the 2012 M_w8.6 Sumatra earthquake, *J. geophys. Res.,* **121**(1), 170–187.

Chorowicz, J., 2005. The East African rift system, *J. Afr. Earth Sci.,* **43**(1–3), 379–410.

Craig, T.J., Jackson, J.A., Priestley, K. & McKenzie, D., 2011. Earthquake distribution patterns in Africa: their relationship to variations in lithospheric and geological structure, and their rheological implications, *Geophys. J Int.,* **185**(1), 403–434.

Domingues, A., Silveira, G., Ferreira, A.M., Chang, S.-J., Custódio, S. & Fonseca, J.F., 2016. Ambient noise tomography of the East African Rift in Mozambique, *Geophys. J Int.,* **204**(3), 1565–1578.

Ebinger, C., Rosendahl, B. & Reynolds, D., 1987. Tectonic model of the Malaŵi rift, Africa, *Tectonophysics,* **141**(1), 215–235.

Fonseca, J.F.B.D. *et al.*, 2014. MOZART: A seismological investigation of the east African rift in central Mozambique, *Seismol. Res. Lett.,* **85**(1), 108–116.

Foster, A.N. & Jackson, J.A., 1998. Source parameters of large African earthquakes: implications for crustal rheology and regional kinematics, *Geophys. J. Int.,* **134**(2), 422–448.

Goldstein, P., Dodge, D., Firpo, M. & Ruppert, S., 1998. What's new in SAC2000? Enhanced processing and database access, *Seismol. Res. Lett.,* **69**(3), 202–205.

Gonzalez-Huizar, H. & Velasco, A.A., 2011. Dynamic triggering: Stress modeling and a case study, *J. geophys. Res.,* **116,** B02304, doi:10.1029/2009JB007000.

Han, L., Peng, Z., Johnson, C.W., Pollitz, F.F., Li, L., Wang, B., Wu, J. & Li, Q., 2017. Shallow microearthquakes near Chongqing, China triggered by the Rayleigh waves of the 2015 M7.8 Gorkha, Nepal earthquake, *Earth, Planets Sci. Lett.,* **479,** 231–240.

Hill, D. & Prejean, S., 2015. Dynamic Triggering, in *Treatise on Geophysics,* 2nd edn, pp. 273–304, ed. Schubert, G., Elsevier.

Hill, D.P. *et al.*, 1993. Seismicity Remotely Triggered by the Magnitude 7.3 Landers, California, Earthquake, *Science,* **260**(5114), 1617–1623.

International Seismological Centre 2016. *On-line Bulletin,* Int. Seismol. Cent., Thatcham, United Kingdom, Available at: http://www.isc.ac.uk.

Kanamori, H. & Brodsky, E.E., 2004. The physics of earthquakes, *Rep. Prog. Phys.,* **67**(8), 1429–1496.

King, G. & Devès, M.. 2015. Fault Interaction, Earthquake Stress Changes, and the Evolution of Seismicity, in *Treatise on Geophysics,* 2nd edn, pp. 243–271, ed. Schubert, G., Elsevier.

Kusky, T.M., Toraman, E., Raharimahefa, T. & Rasoazanamparany, C., 2010. Active tectonics of the Alaotra–Ankay Graben System, Madagascar: Possible extension of Somalian–African diffusive plate boundary?, *Gondwana Res.,* **18**(2–3), 274–294.

McGuire, J.J. & Beroza, G.C., 2012. A Rogue Earthquake Off Sumatra, *Science,* **336**(6085), 1118–1119.

Meng, L., Ampuero, J.-P., Stock, J., Duputel, Z., Luo, Y. & Tsai, V.C., 2012. Earthquake in a maze: compressional rupture branching during the 2012 M_w8.6 Sumatra earthquake, *Science,* **337,** 724–726.

Mougenot, D., Recq, M., Virlogeux, P. & Lepvrier, C., 1986. Seaward extension of the east African rift, *Nature,* **321**(6070), 599–603.

Omori, F., 1894. On the aftershocks of earthquakes, *J. Colloid Sci. Imp. Univ. Tokyo,* **7,** 111–200.

Parsons, T., 2005. A hypothesis for delayed dynamic earthquake triggering, *Geophys. Res. Lett.,* **32,** L04302, doi:10.1029/2004GL021811.

Peng, Z. & Chao, K., 2008. Non-volcanic tremor beneath the Central Range in Taiwan triggered by the 2001 Mw 7.8 Kunlun earthquake, *Geophys. J Int.,* **175**(2), 825–829.

Peng, Z. & Gomberg, J., 2010. An integrated perspective of the continuum between earthquakes and slow-slip phenomena, *Nat. Geosci.,* **3**(9), 599–607.

Peng, Z., Vidale, J.E., Wech, A.G., Nadeau, R.M. & Creager, K.C., 2009. Remote triggering of tremor along the San Andreas Fault in central California, *J. geophys. Res.,* **114,** B00A06, doi:10.1029/2008JB006049.

Pollitz, F.F., Stein, R.S., Sevilgen, V. & Burgmann, R., 2012. The 11 April 2012 east Indian Ocean earthquake triggered large aftershocks worldwide, *Nature,* **490**(7419), 250–253.

Rubinstein, J.L., Vidale, J.E., Gomberg, J., Bodin, P., Creager, K.C. & Malone, S.D., 2007. Non-volcanic tremor driven by large transient shear stresses, *Nature,* **448**(7153), 579–582.

Scholz, C.H., Koczynski, T.A. & Hutchins, D.G., 1976. Evidence for incipient rifting in southern Africa, *Geophys. J. R. astr. Soc.,* **44**(1), 135–144.

Shelly, D.R., Peng, Z., Hill, D.P. & Aiken, C., 2011. Triggered creep as a possible mechanism for delayed dynamic triggering of tremor and earthquakes, *Nat. Geosci,* **4**(6), 384–388.

Singh, M., Kijko, A. & Durrheim, R., 2009. Seismotectonic models for South Africa: synthesis of geoscientific information, problems, and the way forward, *Seismol. Res. Lett.,* **80**(1), 71–80.

Stamps, D.S., Calais, E., Saria, E., Hartnady, C., Nocquet, J.-M., Ebinger, C.J. & Fernandes, R.M., 2008. A kinematic model for the East African Rift, *Geophys. Res. Lett.,* **35,** L05304, doi:10.1029/2007GL032781.

Tape, C., West, M., Silwal, V. & Ruppert, N., 2013. Earthquake nucleation and triggering on an optimally oriented fault, *Earth planet. Sci. Lett.,* **363,** 231–241.

Utsu, T., Ogata, Y. & Matsu'ura, R.S., 1995. The centenary of the Omori formula for a decay law of aftershock activity, *J. Phys. Earth,* **43**(1), 1–33.

van der Elst, N.J., Savage, H.M., Keranen, K.M. & Abers, G.A., 2013. Enhanced remote earthquake triggering at fluid-injection sites in the midwestern United States, *Science,* **341**(6142), 164–167.

Velasco, A.A., Hernandez, S., Parsons, T. & Pankow, K., 2008. Global ubiquity of dynamic earthquake triggering, *Nat. Geosci.,* **1**(6), 375–379.

Wang, W., Meng, X., Peng, Z., Chen, Q.-F. & Liu, N., 2015. Increasing background seismicity and dynamic triggering behaviors with nearby mining activities around Fangshan Pluton in Beijing, China, *J. geophys. Res.,* **120**(8), 5624–5638.

Wei, S., Helmberger, D. & Avouac, J.-P., 2013. Modeling the 2012 Wharton basin earthquakes off-Sumatra: complete lithospheric failure, *J. geophys. Res.,* **118**(7), 3592–3609.

Wessel, P. & Smith, W. H.F., 1998. New, improved version of generic mapping tools released, *EOS, Trans. Am. geophys. Un.,* **79**(47), 579.

Wu, J., Peng, Z., Wang, W., Gong, X., Chen, Q. & Wu, C., 2012. Comparisons of dynamic triggering near Beijing, China following recent large earthquakes in Sumatra, *Geophys. Res. Lett.,* **39,** L21310, doi:10.1029/2012GL053515.

Yue, H., Lay, T. & Koper, K.D., 2012. En echelon and orthogonal fault ruptures of the 11 April 2012 great intraplate earthquakes, *Nature,* **490**(7419), 245–249.

Zhang, Q., Lin, G., Zhan, Z., Chen, X., Qin, Y. & Wdowinski, S., 2017. Absence of remote earthquake triggering within the Coso and Salton Sea geothermal production fields, *Geophys. Res. Lett.,* **44**(2), 726–733.

SUPPORTING INFORMATION

Supplementary data are available at *GJI* online.

Figure S1. The absence of triggering in 23 stations located near structures of the EARS during the passage of seismic waves generated by the M_w8.6 2012 Indian Ocean main shock. Envelope of the high-pass filtered (≥5 Hz) waveforms (black) and raw three-component waveform at TETE station (light blue).

Figure S2. The absence of remote dynamic triggering at station MBAR in Uganda, EARS Western Branch. Same caption as for Fig. 3. At this station waveforms were high-pass filtered (≥5 Hz). The detected increase in activity is not statistically significant.

Figure S3. The absence of remote dynamic triggering at station LODK in Kenya, EARS Eastern Branch. Same caption as for Fig. 3. At this station waveforms were high-pass filtered (≥5 Hz). Although some activity was detected during and after the surface wave train, it is similar to the activity detected before.

Table S1. Details of the 53 analysed stations. Stations with strong noise in the frequency band of interest are marked with *. Stations of the MOZART temporary deployment are marked with network code (Moz).

Please note: Oxford University Press is not responsible for the content or functionality of any supporting materials supplied by the authors. Any queries (other than missing material) should be directed to the corresponding author for the paper.